scientific reports

Check for updates

OPEN

Geometric working volume of a satellite positive displacement machine

Pawel Sliwinski

This article describes a method for determining the geometric working volume of satellite positive displacement machines (pump and motor). The working mechanism of these machines is satellite mechanism consisting of two non-circular gears (rotor and curvature) and circular gears (satellites). Two variants of the satellite mechanism are presented. In the first mechanism, the rolling line of the rotor is a sinusoid "wrapped" around a circle. In the second mechanism, the rolling line of the rotor is a double sinusoid "wrapped" around a circle. A method for calculating the area of the working chamber as a function of the rotor rotation angle is presented, based on mathematical formulae of the rotor, the curvature and the satellite rolling lines. It has been shown that the second variant of the satellite mechanism is advantageously characterised by a larger difference between the maximum area of the working chamber and the minimum area of this chamber. New mathematical formulas have been proposed to calculate the area of the working chamber for any angle of rotation of the shaft (rotor) based on the maximum and minimum values of the area of this chamber. It was thus confirmed that the geometric working volume depends on the maximum and minimum area of a working chamber and on the height of the satellite mechanism. The analyses of the area of the working chamber were carried out both for the mechanism without gears (the area delimited by the rolling lines of the elements of the mechanism) and for the real mechanism with gears. Differences in the values of these fields were also detected.

Keywords Working volume, Geometric working volume, Non-circular mechanism, Satellite mechanism, Pump, Motor, Satellite, Rotor, Curvature, Positive displacement, Energy efficiency, Discharge machining

Every hydraulic positive displacement machine, i.e. a pump and a hydraulic motor, is characterised by the fact that a ceertain amount of fluid flows through its working mechanism during the rotation of the shaft. Therefore, the working mechanism of positive displacement machines is designed in such a way that the process of filling and emptying of working chambers of this mechanism takes place during the rotation of the shaft. The filling and emptying process is only possible if the volume of the working chambers changes cyclically. Therefore, in every positive displacement machine, each working chamber must change its volume from the minimum V_{min} to the maximum V_{max}.

The sum of the volume changes ΔV_{ch} of all chambers of the working mechanism per one full revolution of the machine shaft is referred to as the geometric working volume q_g, often called the working volume for short. This is the most important parameter that indicates the size of the displacement machine (pump or hydraulic motor). The unit of geometric working volume is m^3/rev. In most cases, however, e.g. in catalogues of displacement machines, cm^3/rev is specified. The geometric working volume can be given in the following form:

$$q_g = n_{ch} \cdot \Delta V_{ch} \tag{1}$$

where:

- n_{ch} – the number of cycles (filling and emptying) of the working chambers per one revolution of the shaft;
- ΔV_{ch} – the change in the volume of a working chamber, calculated from the drawing documentation of the working mechanism as:

$$\Delta V_{ch} = V_{ch-max} - V_{ch-min} \tag{2}$$

Faculty of Mechanical Engineering and Ship Technology, Gdansk University of Technology, Gabriela Narutowicza 11/12 Str, 80-233 Gdansk, Poland. email: pawel.sliwinski@pg.edu.pl

- $V_{k\text{-}max}$ – the maximum volume of a working chamber (Fig. 1),
- $V_{k\text{-}min}$ – the minimum volume of a working chamber (Fig. 1).

The volume of the working chamber V_{ch} and thus the geometric working volume q_g of the positive displacement machine is determined on the basis of the design documentation of this machine (as in[1,2]) or on the basis of precise measurements of the elements of the working mechanism. Moreover, the geometric working volume q_g is not the theoretical working volume q_t. In articles[3–5] it was shown that the geometric working volume q_g differs from the theoretical working volume q_t. It was also shown that it depends on the pressure difference Δp_i in the working chambers, i.e. the pressure difference Δp_i causes elastic deformation of these chambers and thus an increase in their volume. The so-called actual working volume q_r was defined in this way. This volume should be used to calculate the volumetric, mechanical and pressure efficiency. However, neither the geometric working volume q_g nor the theoretical working volume q_t should be used to calculate these efficiencies[3–5].

According to[3–6], the theoretical working volume should be understood as the amount of fluid flowing in the positive displacement machine during one complete revolution without volume losses (and therefore with $\Delta p_i = 0$) and in the absence of other phenomena affecting this flow. So far, however, a simplification has been used and the theoretical working volume or even the geometric working volume is used to calculate the above-mentioned partial efficiencies, as for example in[7–12]. In this way the geometric working volume, albeit incorrectly, is identified with the theoretical working volume, as for example in[13]. In the literature, for example in[2,14–17], there is a very general concept, namely specific absorption.

It is desirable that for a given geometric working volume q_g the change in the volume ΔV_{ch} of the working chamber is maximal. Then a working mechanism with a lower height H and therefore lower mass is obtained. In this way, a favourably lower mass M of the positive displacement machine is achived.

The subject of this article is the geometric working volume of a positive displacement machine, whose working mechanism is the so-called satellite mechanism (Fig. 1). The structure and operation principle of this mechanism have been described in many publications, including[3–5,18–26] and the method of its construction in[14,25,26]. It should be remembered that in these mechanisms, the volume V_{ch} of the chamber changes from the $V_{ch\text{-}min}$ to the $V_{ch\text{-}max}$ during the rotation of the rotor. These volumes are expressed by formulae[6]:

$$V_{ch-max} = H \cdot A_{ch-max} \tag{3}$$

$$V_{ch-min} = H \cdot A_{ch-min} \tag{4}$$

where:

- H – the height of the mechanism,
- $A_{ch\text{-}max}$ – the area of the working chamber with the maximum volume (Fig. 1),
- $A_{ch\text{-}min}$ – the area of the working chamber with the minimum volume (Fig. 1).

The change in the volume of the working chamber is therefore:

$$\Delta V_{ch} = H \cdot \Delta A_{ch} \tag{5}$$

$$\Delta A_{ch} = A_{ch-max} - A_{ch-min} \tag{6}$$

During one complete rotation of the rotor (360° rotation), the volume of all working chambers changes in the following number of cycles[6,14]:

$$n_{ch} = n_C \cdot n_R \tag{7}$$

where:

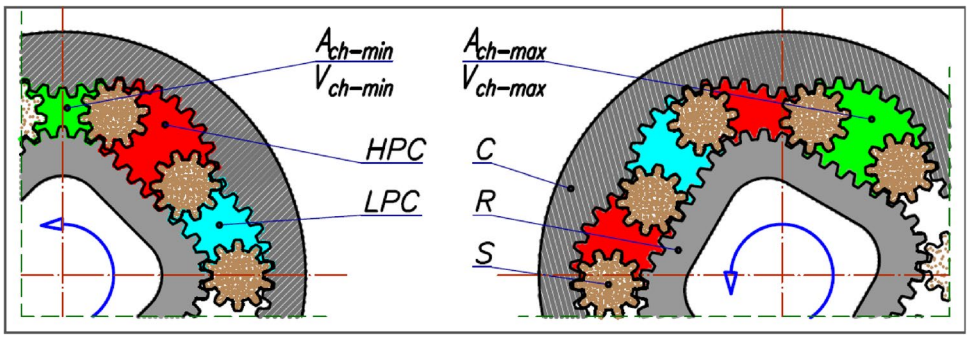

Figure 1. Satellite mechanism type 4×6: C curvature, R rotor, S satellite, HPC high-pressure working chamber, LPC low-pressure working chamber [38,39].

- n_C – the number of curvature humps,
- n_R – the number of rotor humps.

Therefore, the geometric working volume q_g of the satellite mechanism is calculated according to the following formula[3–6]:

$$q_g = n_{ch} \cdot \Delta V_{ch} \tag{8}$$

The most important parameters for the calculation of the geometric working volume q_g are thus the areas of the working chambers $A_{ch\text{-}max}$ and $A_{ch\text{-}min}$. The first attempts to calculate these areas were made by Kujawski and Drogosz[2,14–17]. However, they referred a satellite mechanism with a three-hump rotor and a four-hump curvature (3 × 4 type mechanism as in[27–30]). The article[15] presents general equations for calculating the "specific absorption" of a motor with a 3 × 4 type satellite mechanism:

$$q_g = 0.5 \cdot H \cdot n_C \cdot n_R \cdot \int_{\alpha_{R-min}}^{\alpha_{R-max}} (r_{R-1} \cdot r_{E-1} - r_{R-2} \cdot r_{E-2}) \cdot d\alpha_R \tag{9}$$

where:

- α_R – the angle of rotation of the rotor;
- $\alpha_{R\text{-}min}$ – the angle of rotation of the rotor corresponding to the working chamber with $A_{ch\text{-}min}$;
- $\alpha_{R\text{-}max}$ – the angle of rotation of the rotor corresponding to the working chamber with $A_{ch\text{-}max}$;
- $r_{R\text{-}1}$ – the distance from the axis of the rotor to the point of contact of the first satellite with the rotor;
- $r_{R\text{-}2}$ – the distance from the axis of the rotor to the point of contact of the second satellite with the rotor (adjacent to the first satellite);
- $r_{E\text{-}1}$ – the distance from the axis of the rotor to the point of contact of the first satellite with the curvature;
- $r_{R\text{-}2}$ – the distance from the axis of the rotor to the point of contact of the second satellite with the curvature (adjacent to the first satellite).

The above formula is therefore based on the equations of the rolling lines of the rotor and curvature and is therefore valid for a satellite mechanism without teeth. In[16] a simplified function is presented that describes the rolling line of the rotor of this mechanism (3 × 4) in polar coordinates:

$$r_R = a \cdot \left(1 - p \cdot \cos(n_R \cdot \alpha_R)\right) \tag{10}$$

where a and p are constants. The equations for the curvature rolling line were not disclosed. In[16] an attempt was made to compare the obtained result of the calculations of the change ΔA_{ch} in the field of the working chamber with the results of the planimeter and with the results for the real motor (with a geared mechanism), but he did not explain how he measured the areas of the chambers of the real mechanism. The differences reached almost 3%. However, in[17] the results of the first calculations of the "specific absorption" of various satellite motors using the AutoCAD programme were presented. In this program, the pitch lines of the mechanism were drawn, a mechanism (without teeth) was created and the $A_{ch\text{-}max}$ and $A_{ch\text{-}min}$ areas of the working chambers were determined. The issues of areas and "specific absorption" were dealt with in a similar way in[2]. This paper also proposes a mathematical formula for calculating the A_{ch} area of the working chamber as a function of the rotor rotation angle α_R. This formula is described in Sect. 6.1.

In [26] it was proposed to calculate the area of the working chamber of a 4 × 6 satellite mechanism for any rotor rotation angle α_R. However, this is a very general proposal, as the authors presented a mathematical formula to describe the rotor pitch line but did not provide a formula to calculate the pitch line of the curvature (similarly as in[16]). Therefore, it is not possible to calculate the area under the pitch line of the curvature in a simple analytical way. It is also not specified according to which function the value of the working chamber changes depending on the rotor rotation angle α_R from $A_{ch\text{-}min}$ to $A_{ch\text{-}max}$. However, they suggest calculating the working volume of the 4 × 6 type satellite mechanism using the following empirical formula (approximate formula)[26]:

$$q_g = \frac{1}{20} \cdot H \cdot m^2 \cdot \left(\frac{z_R}{n_R} - z_S\right)^2 \cdot \left(1.433 \cdot \left(\frac{n_R \cdot z_S}{z_R - n_R \cdot z_S}\right)^{1.481} + 2.144\right) \tag{11}$$

where:

- m—The tooth modulus,
- z_S—The number of teeth on the satellite,
- z_R—The number of teeth on the rotor.

The above formula only applies to only for the 4 × 6 satellite mechanism, in which the pitch line of the rotor is described by the high-order ellipses. Therefore, the above formula does not work for mechanisms with a different rotor curve.

The methods previously known in the literature for calculating the working volume of a satellite machine referred to the calculation of this volume in a 3 × 4 type satellite mechanism. Furthermore, these methods were based on the determination of the $A_{ch\text{-}max}$ and $A_{ch\text{-}min}$ areas of the working chambers, which are generated by

the pitch lines of the rotor, the curvature and the satellites. Therefore, the areas for the real mechanism, i.e. the toothed mechanism, were not calculated.

Therefore, there is no information in the literature about the differences in the values of the $A_{ch\text{-}max}$ and $A_{ch\text{-}min}$ areas of the working chambers of toothed and non-toothed mechanisms and how the number of teeth in the mechanism affects the above-mentioned areas. Furthermore, the publication [2] does not state whether the proposed mathematical formula for calculating the working chamber area A_{ch} as a function of the rotor rotation angle α_R is suitable for calculating the chamber area of a real (i.e. toothed) mechanism and, if so, with what error. The aim of this article is therefore to dispel the above-mentioned doubts and to propose a new mathematical formula for calculating the area A_{ch} of the working chamber as a function of the rotor rotation angle α_R. Positive displacement machines with a 3 × 4 satellite mechanism are no longer manufactured (mainly because of the small number of working chambers and the hydrostatic imbalance (as a result of the pressure in the working chambers, the shaft is bent and the bearings are heavily loaded)). This article therefore analyses the latest 4 × 6 satellite mechanisms.

New construction of satellite mechanisms

According to the methodology described in[14], two variants of the 4 × 6 satellite mechanism were developed, i.e.:

1) first variant (I) (Fig. 2) – the rotor pitch line is described by the following equation[22]:

$$R = \frac{D}{2} - A \cdot \cos(n_R \cdot \alpha) \tag{12}$$

2) second variant (II) (Fig. 3) – the rotor pitch line is described by[23]:

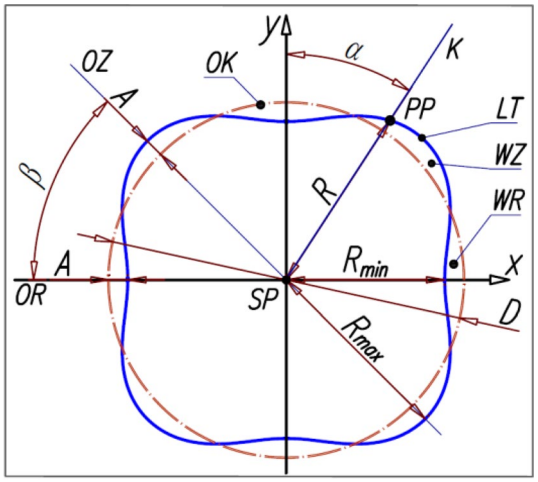

Figure 2. Parameters of the rotor pitch line of the 4 × 6 type satellite mechanism – variant I: K the half-line with the origin in the centre SP of the rotor rotation and passig through the point PP on the pitch line LT, WZ – the hump convexity, WR the hump concavity, OK circle with diameter D, OZ the axis of symmetry of the hump convexity, OR the axis of symmetry of the hump concavity, PP point of intersection of the half-line K with the pitch line LT, β —The angle between the axis OR and the axis OZ. Other designations in the tekst [22].

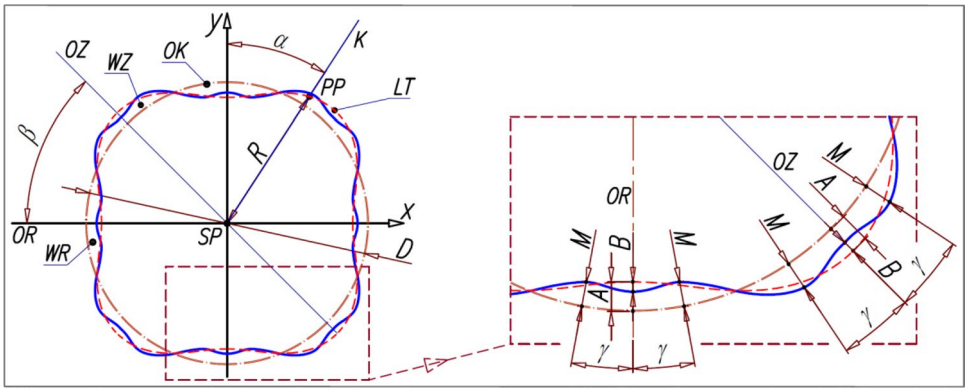

Figure 3. Parameters of the rotor pitch line of the 4 × 6 type satellite mechanism—variant II. Designations as in Fig. 2 and in the text [23].

$$R = \frac{D}{2} - A \cdot cos(n_R \cdot \alpha) + B \cdot cos(2 \cdot n_R \cdot \alpha) \tag{13}$$

where (Fig. 2 and Fig. 3):

D – the diameter of the base circle OK of the rotor,

α – the angle with the origin in the centre SP of the rotor rotation and with the arms formed by any axis of the XY coordinate system and the line K,

A – the distance of the point PP from the circle OK for B = 0, which lies in the axis of symmetry OZ of the hump convexity WZ and in the axis of symmetry OR of the hump concavity WR,

B – the amount by which the distance of the point P from the circle OK is reduced.

If $B \geq \frac{A}{4}$, then the maximum distance M of the point PP from the circle OK is to the left and right of the axis OZ of the hump convexity WZ and to the left and right of the axis OR of the hump concavity WR, at the distance of the angle γ from these axes, where[23]:

$$\gamma = \frac{1}{n_R} \cdot \arccos\left(\frac{A}{n_R \cdot B}\right) \tag{14}$$

If $B < \frac{A}{4}$, then the maximum distance M of the point PP from the circle OK lies in the axis of symmetry OZ of the hump convexity WZ and in the axis of symmetry OR of the hump concavity WR and for the hump convexity WZ is[23]:

$$M = R - \frac{D}{2} \tag{15}$$

However, for the hump concavity WR is[23]:

$$M = \frac{D}{2} - R \tag{16}$$

The large pressure difference acting on the satellite causes high pressures in the area of the interacting teeth of the mechanism elements[20] and high bending stresses in the tooth root. It is therefore recommended to use as few teeth as possible on the satellite, which makes the tooth thicker. In typical gears, the minimum limit number of teeth is 17, below which undercutting of the tooth root occurs[31]. If slight undercutting is allowed, the minimum limit number of teeth can be 14[31]. To increase the durability of the teeth of the satellite mechanism, it was decided to use satellites with a very low number of teeth, i.e. 10 or less[14,21–23,32,33]. For example:

- In [21] and in a satellite mechanism is presented in which the satellite has 10 teeth;
- In [22,23,32] a satellite mechanism is presented in which the satellite has 9 teeth;
- In [14] a satellite mechanism is presented in which the satellite has 8 teeth;
- In [33] a satellite mechanism is presented in which the satellite has 5 teeth and these are teeth with a circular-arch shape.

Then, in order to avoid undercutting the tooth root, both the head and the root are low. This means that both the height h_a of the tooth head and the height h_f of the tooth root are smaller than the tooth modulus m (Table 1).

Considered satellite mechanisms

In this article, satellite mechanisms according to the patent descriptions[22,23] are considered, where the number of satellite teeth is 9 and 14 (Fig. 4 and Fig. 5). The parameters of these mechanisms are listed in Table 1, Table 2 and Fig. 6. When designing these mechanisms, the aim was to maximise the values of parameters A and B (Table 1) while complying with the conditions described in[14] in order to obtain the largest possible geometric working volume q_g.

Area of the working chamber

Methods for determining the area of the working chamber

Figure 1 and Fig. 4 show the location of the satellite mechanismu for which the minimum A_{min} and the maximum A_{max} area of the working chamber are determined (Figs. 6 and 7 shows the minimum and maximum areas of the working chamber, which were determined using the CAD documentation based on the pitch lines of the mechanism elements ($A_{ch\text{-}P\text{-}min}$ and $A_{ch\text{-}P\text{-}max}$) and the real areas (toothed elements – ($A_{ch\text{-}S\text{-}min}$ and $A_{ch\text{-}S\text{-}max}$).

The area A_{ch} of the working chamber for any angle α_R of the rotor rotation can be determined in two ways, namely:

1) by direct reading from the documentation of the working mechanism in the CAD programme;
2) analytical method – by setting up the mathematical formula $A_{ch} = f(R,\alpha_R)$.

The first method is very easy and quick to use, and all the areas of the working chambers were calculated in this way.

The second method requires knowledge of mathematical functions that describe the edges of the area. In the case of real areas of working chambers, i.e. toothed areas, finding such functions is very difficult (due to the complicated geometry of the teeth and their orientation in the coordinate system). For this reason, the analytical

parameters common to variants I and II				
n_R	n_E	z_s	z_R	z_E
4	6	9	40	60
$D_{p\text{-}S}$	$D_{r\text{-}S}$	$A_{p\text{-}S}$	$H_{a\text{-}S}$	$H_{f\text{-}S}$
9 mm	8.84816 mm	30°	0.855 mm	0.900 mm
m	β	$h_{a\text{-}CH}$	$h_{f\text{-}CH}$	–
1.0 mm	45°	0.900 mm	0.857 mm	–
correction coef. of the satellite and chisel teeth			Δh_a	Δh_f
x = – 0.07592			0.045	0.043 mm
parameters for mechanism of variant I				
A	D	–	–	–
1.6663 mm	38.8795 mm	–	–	–
parameters for mechanism of variant II				
A	B	D	M	γ
2.3478 mm	0.41086 mm	37.5648 mm	1.937 mm	–
Areas of the satellite S and chisel CH (in mm^2) (Fig. 6)				
	A_a	A_f	$A_{a\text{-}S\text{-}CH}$	$A_{f\text{-}S\text{-}CH}$
Satellite S	0.9226	0.9395	0.0182	0.0258
Chisel CH	0.9408	0.9137		

Table 1. Basic parameters of the satellite mechanisms with the nine-toothed satellite. The subscript "CH" refers to the chisel.

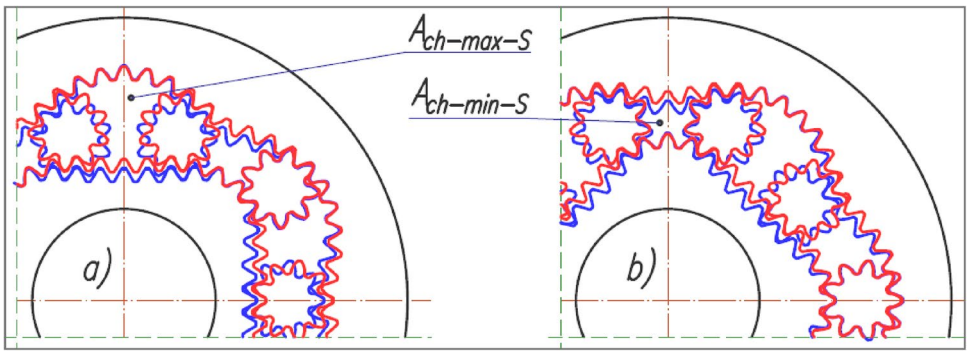

Figure 4. Satellite mechanism with nine-toothed satellite—variant I (red colour) and variant II (blue colour): (**a**) comparison of the maximum area $A_{ch\text{-}max}$ of the working chamber of these mechanisms; (**b**) comparison of the minimum area $A_{ch\text{-}min}$ of the working chamber of these mechanisms.

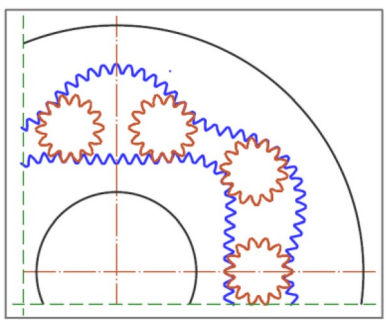

Figure 5. Satellite mechanism variant II with fourteen-toothed satellite.

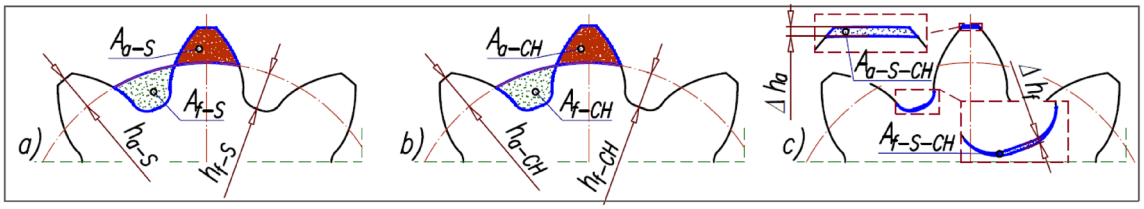

Figure 6. Areas of the satellite (**a**), the chisel (**b**) and the difference between the areas of the chisel and the satellite (**c**).

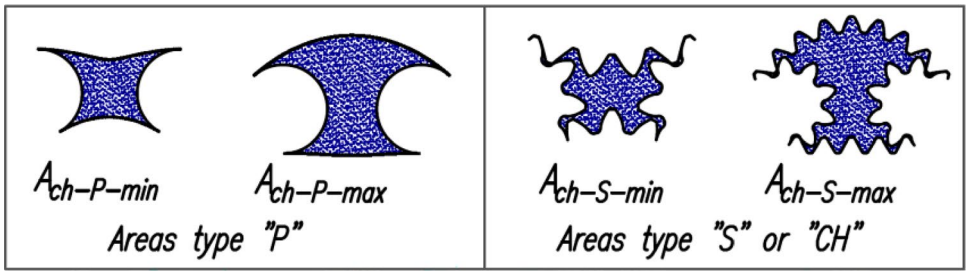

Figure 7. Minimum and maximum areas of the working chamber determined from the CAD documentation on the basis on the pitch lines of the mechanism elements and the real areas (toothed elements).

method can be limited to determining the areas of the working chambers, the edges of which are the pitch lines of the rotor teeth, the curvature teeth and satellites teeth. The pitch line of the rotor is described by the formula (12) or (13). However, the pitch line of the curvature is determined by a series of points (x_E,y_E), whose values are calculated according to the method described in[19]. Therefore, the pitch line of the curvature cannot be described by a simple mathematical formula.

The area of the working chamber is:

$$A_{ch} = A_C - A_R - A_{S1} - A_{S2} \tag{17}$$

where:

$$A_C = \frac{1}{2} \cdot \int_{\varphi_1}^{\varphi_2} (f_C)^2 d\varphi = \frac{1}{2} \cdot \sum_{i=1}^{n} \left({R_E}^{(i)} \cdot \Delta {L_E}^{(i)} \right) \tag{18}$$

A_C – the area bounded by the pitch line of the curvature (between points $E^{(1)}$ and $E^{(2)}$):

$R_E^{(i)}$ – the distance from the centre of the mechanism to point $E^{(i)}$ on the curvature (the radius of the curvature);

$\Delta L_E^{(i)}$ – the length of the „i"-th elementary section of the curvature pitch line, calculated according to the method described in[14];

n – the number of elementary sections of the curvature pitch line between the points $E^{(1)}$ and $E^{(2)}$;

A_R – the area bounded by the rotor pitch line (between the points $F^{(1)}$ and $F^{(2)}$):

$$A_C = \frac{1}{2} \int_{\varphi_1}^{\varphi} (f_R)^2 d\varphi \tag{19}$$

$$f_R = \frac{D}{2} - A \cos\left(n_R (\alpha + \alpha_R)\right) \tag{20}$$

or

$$f_R = \frac{D}{2} - A \cdot \cos(n_R \cdot (\alpha + \alpha_R)) + B \cdot \cos(2 \cdot n_R \cdot (\alpha + \alpha_R)) \tag{21}$$

f_R—The function that describes the rotor pitch line after it has been rotated by an angle α_R:

A_{S1}—The area of a fragment of a satellite centred on the point $S^{(1)}$;

κ_1—The central angle of a satellite centred on the point $S^{(1)}$ in deg;

A_{S2}—The area of a fragment of a satellite centred on the point $S^{(2)}$:

κ_2—The central angle of a satellite centred on the point $S^{(2)}$ in deg.

$$A_{S1} = \frac{D_{p-S}^2}{4} \left(1 - \frac{\kappa_1}{360} + \frac{\sin \kappa_1}{2} \right) \tag{22}$$

n_R	n_E	z_S	z_R	z_E
4	6	14	64	96
$D_{p\text{-}s}$	$D_{r\text{-}s}$	$\alpha_{p\text{-}S}$	$H_{a\text{-}s}$	$H_{f\text{-}s}$
9 mm	9.10 mm	30°	0.5496 mm	0.810 mm
m	x	β	$H_{a\text{-}CH}$	$H_{f\text{-}CH}$
0.643 mm	0.0785	45°	0.5786 mm	0.7662 mm
Correction coef. of the satellite and chisel teeth			Δh_a	Δh_f
x = 0.0785			0.029	0.0438 mm
Areas of the satellite S and chisel CH (in mm^2) (Fig. 6)				
	A_a	A_f	$A_{a\text{-}s\text{-}CH}$	$A_{f\text{-}S\text{-}CH}$
Satellite S	0.3805	0.4882	0.0084	0.0184
Chisel CH	0.3889	0.4698		

Table 2. Basic parameters of the satellite mechanisms variant II with the fourteen-toothed satellite. The subscript "CH" refers to the chisel.

$$A_S 2 = D_{(p-S)^2}/4\,(1 - \kappa_2/360 + \sin\,\kappa_2/2) \tag{23}$$

In[2] and[26] it was shown that the area of the working chamber of the satellite mechanism is directly proportional to the square of the tooth modulus. It is obvious that the pitch diameter of the satellite is also proportional to the number of teeth. Therefore, we can assume that the following relationship is true:

$$A_{ch} = C_{ch} \cdot m^2 \cdot {z_S}^2 \tag{24}$$

where C_{ch} is a proportionality coefficient that depends on the type of satellite mechanism and the geometrical parameters of this mechanism (as in Table 1 and Table 2). This coefficient also depends on whether we consider a non-toothed or a toothed chamber. Moreover, this coefficient takes values from $C_{ch\text{-}min}$ to $C_{ch\text{-}max}$ for a chamber whose area varies between $A_{ch\text{-}min}$ and $A_{ch\text{-}max}$.

The values of the areas of the working chamber

Table 3 shows the minimum and maximum values of the working chamber area for both variants of the satellite mechanism and for:

a) the real (toothed) satellite mechanism – $A_{ch\text{-}S\text{-}min}$ and $A_{ch\text{-}S\text{-}max}$ areas;
b) the backlash-free mechanism (that is the satellite is a chisel – as in Fig. 6b) – $A_{ch\text{-}CH\text{-}min}$ and $A_{ch\text{-}CH\text{-}max}$ areas;
c) the areas determined by the pitch line of the rotor, the curvature and the satellites – $A_{ch\text{-}P\text{-}min}$ and $A_{ch\text{-}P\text{-}max}$ areas;
d) the number of teeth on the satellite 9 and 14 respectively – in variant II of the mechanism (Fig. 8).

Table 3 are also shows the relative differences in the areas of the working chamber for variants I and II of the mechanism, calculated as:

$$\delta A_{ch-I-II} = \left(\frac{A_{ch-II}}{A_{ch-I}} - 1\right) \cdot 100 \tag{25}$$

and the relative differences in the areas of the working chambers in variant II of the mechanism for a satellite with 9 and 14 teeth and calculated as:

$$\delta A_{ch-9-14} = \left(\frac{A_{ch-14}}{A_{ch-9}} - 1\right) \cdot 100 \tag{26}$$

		$A_{ch\text{-}P\text{-}min}$	$A_{ch\text{-}P\text{-}max}$	$A_{ch\text{-}S\text{-}min}$	$A_{ch\text{-}S\text{-}max}$	$A_{ch\text{-}CH\text{-}min}$	$A_{ch\text{-}CH\text{-}max}$
Variant I		48.7266	108.9258	48.3736	108.3422	47.9652	107.9052
Variant II	9 teeth	32.7636	120.5814	33.2226	121.0698	32.9421	120.6625
	14 teeth			33.4174	121.6259	33.4001	121.3398
$\delta A_{ch\text{-}I\text{-}II}$	9 teeth	−32.76%	10.70%	−31.32%	11.75%	−31.32%	11.75%
	14 teeth			−30.92%	12.26%	−30.36%	12.45%
$\delta A_{ch\text{-}9\text{-}14}$		–	–	0.58%	0.46%	1.39%	0.56%

Table 3. Minimum and maximum area of the working chamber in mm2.

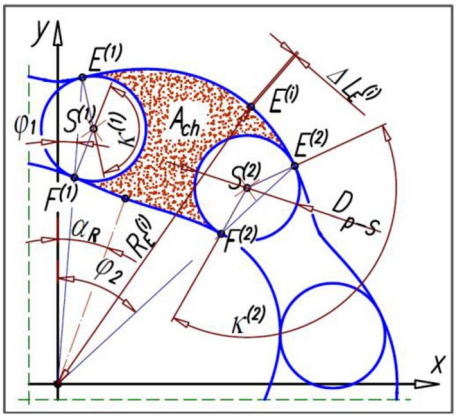

Figure 8. Area A_{ch} of the working chamber with characteristic points for each angle α_R of the rotor rotation.

Table 4 Shows the relative differences in the above-mentioned areas, calculated as follows:

$$\delta A_{ch-P-S} = \left(\frac{A_{ch-S}}{A_{ch-P}} - 1\right) \cdot 100 \tag{27}$$

$$\delta A_{ch-P-CH} = \left(\frac{A_{ch-CH}}{A_{ch-P}} - 1\right) \cdot 100 \tag{28}$$

$$\delta A_{ch-S-CH} = \left(\frac{A_{ch-CH}}{A_{ch-S}} - 1\right) \cdot 100 \tag{29}$$

$$\delta\left(\Delta A_{ch-P-I-II}\right) = \left(\frac{\Delta A_{ch-P-II}}{\Delta A_{ch-P-I}} - 1\right) \cdot 100 \tag{30}$$

$$\delta\left(\Delta A_{ch-S-I-II}\right) = \left(\frac{\Delta A_{ch-S-II}}{\Delta A_{ch-S-I}} - 1\right) \cdot 100 \tag{31}$$

$$\delta\left(\Delta A_{ch-CH-I-II}\right) = \left(\frac{\Delta A_{ch-CH-II}}{\Delta A_{ch-CH-I}} - 1\right) \cdot 100 \tag{32}$$

$$\delta\left(\Delta A_{ch-P-S}\right) = \left(\frac{\Delta A_{ch-S}}{\Delta A_{ch-P}} - 1\right) \cdot 100 \tag{33}$$

$$\delta\left(\Delta A_{ch-P-CH}\right) = \left(\frac{\Delta A_{ch-CH}}{\Delta A_{ch-P}} - 1\right) \cdot 100 \tag{34}$$

$$\delta\left(\Delta A_{ch-S-CH}\right) = \left(\frac{\Delta A_{ch-CH}}{\Delta A_{ch-S}} - 1\right) \cdot 100 \tag{35}$$

Figure 9 shows the characteristics of the areas of the working chamber of the mechanism of variant II and the relative differences depending on the angle α_R of rotation of the rotor for all the option mentioned above, i.e. according to the pitch line, the real mechanism (toothed) and the backlash-free mechanism (satellite = chisel) (Table 5).

		$\delta A_{ch\text{-}P\text{-}S\text{-}min}$	$\delta A_{ch\text{-}P\text{-}S\text{-}max}$	$\delta A_{ch\text{-}P\text{-}CH\text{-}min}$	$\delta A_{ch\text{-}P\text{-}CHmax}$	$\delta A_{ch\text{-}S\text{-}CH\text{-}min}$	$\delta A_{ch\text{-}S\text{-}CH\text{-}max}$
Variant I		− 0.73	− 0.54	− 1.56	− 0.94	− 0.85	− 0.40
Variant II	9 teeth	1.40	0.40	0.54	0.07	− 0.85	− 0.34
	14 teeth	2.0	0.87	–	–	–	–

Table 4. Relative differences (in %) of the areas Ach-max and Ach-min of the working chamber.

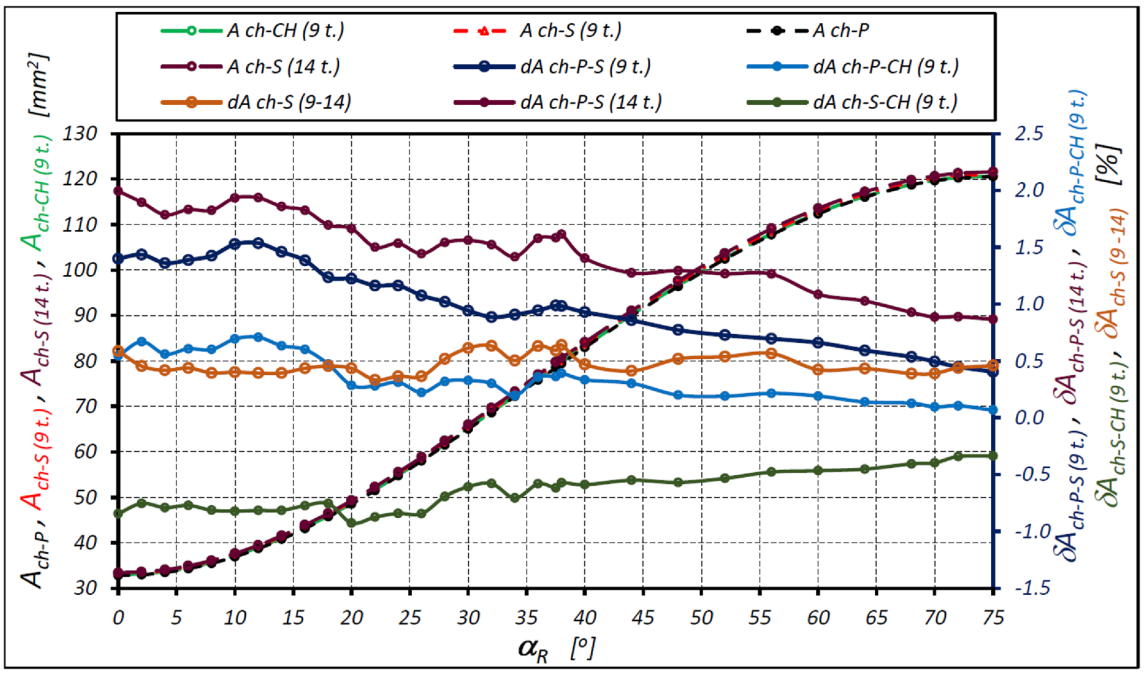

Figure 9. Areas A_{ch} of the working chamber as a function of the angle α_R of the rotor rotation: $A_{ch\text{-}P}$ – the area created by the pitch line of the rotor, the curvature and the satellites; $A_{ch\text{-}S\,(9\,t.)}$ – the area of the toothed chamber for $z_S = 9$; $A_{ch\text{-}S\,(14\,t.)}$ – the area of the toothed chamber for $z_S = 14$; $A_{ch\text{-}CH\,(9\,t.)}$ – the area of the toothed chamber for $z_S = 9$ (backlash-free mechanism); $\delta A_{ch\text{-}P\text{-}S\,(9\,t.)}$ – the relative difference between the areas of $A_{ch\text{-}P}$ and $A_{ch\text{-}S\,(9\,t.)}$; $\delta A_{ch\text{-}P\text{-}S\,(14\,t.)}$ – the relative difference between the areas of $A_{ch\text{-}P}$ and $A_{ch\text{-}S\,(14\,t.)}$; $\delta A_{ch\text{-}P\text{–}CH\,(9\,t.)}$ – the relative difference between the areas of $A_{ch\text{-}P}$ and $A_{ch\text{-}CH\,(9\,t.)}$; $\delta A_{ch\text{-}S\text{-}CH\,(9\,t.)}$ – the relative difference between the areas of $A_{ch\text{-}S}$ and $A_{ch\text{-}CH\,(9\,t.)}$; $\delta A_{ch\text{-}S\,(9\text{–}14)}$ – the relative difference between the areas of $A_{ch\text{-}S\,(9\,t.)}$ and $A_{ch\text{-}S\,(14\,t.)}$.

		$\Delta A_{ch\text{-}P}$	$\Delta A_{ch\text{-}S}$	$\Delta A_{ch\text{-}CH}$	$\Delta(\Delta A_{ch\text{-}P\text{-}S})$	$\Delta(\Delta A_{ch\text{-}P\text{-}CH})$	$\Delta(\Delta A_{ch\text{-}S\text{-}CH})$
Variant I		60.1992	59.9686	59.940	−0.38%	− 0.43%	−0.05%
Variant II	9 teeth	87.8178	87.8472	87.7204	0.03%	− 0.11%	−0.14%
	14 teeth		88.2085	–	0.44%	–	–
$\delta(A_{ch\text{-}I\text{-}II})$	9 teeth	45.87%	46.49%	46.35%	–	–	–
	14 teeth		47.22%	–	–	–	–

Table 5. Differences of the maximum and minimum areas (in mm2) and their relative differences (in %).

The comparative index of a positive displacement machine

The power density

Some scientists, dealers and manufacturers of hydraulic positive displacement machines use the term "power density" for comparative and marketing purposes. This "power density" ρ_P is understood as the ratio of the nominal mechanical power P_M of the positive displacement machine to its mass M_M, i.e.[34–37]:

$$\rho_P = \frac{P_M}{M_M} \tag{36}$$

However, in [26] the power density ρ_P for satellite machines was defined as:

$$\rho_P = \frac{q_g}{\pi \cdot {R_{Cmax}}^2 \cdot H} \tag{37}$$

where R_{Cmax} is the maximum value of the radius of the pitch line of the curvature.

The above definitions are characterised by a certain imprecision. In the case of formula (36), the mechanical power P_M of the machine is a function of the speed of its shaft. Therefore, it is difficult to compare different types of positive displacement machines, because with the same nominal power, the different machines have different nominal rotational speed and different nominal torque. However, formula (37) only indicates the geometric working volume q_g that can be accommodated in a cylinder of radius R_{Cmax} and height H. There is therefore no indication of the total mass M_M of the device.

Specific mass of the positive displacement machine

In the context of the inaccuracies described above, a new comparative index for positive displacement machines is proposed, which is defined as follows:

$$\rho_q = \frac{M_M}{q_g} \tag{38}$$

This index is proposed to denote the specific mass of the positive displacement machine. Logic dictates that the value of this indicator should be compared for machines with the same or similar nominal working pressure p_{nom}.

Models of the working chamber area as a function of the rotor rotation angle

The know model of the working chamber area

According to[2] the area A_{ch} of the working chamber of a satellite mechanism changes as a function of the rotor rotation angle α_R according to the following relationship:

$$A_{ch} = 0.5 \cdot \left(A_{ch-max} - A_{ch-min}\right) \cdot (1 - \cos(\alpha_R \cdot n_{CR})) + A_{ch-min} \tag{39}$$

where:

$$n_{CR} = \frac{n_C \cdot n_R}{n_C + n_R} \tag{40}$$

Figure 10 shows the characteristics of the areas of the working chamber of the mechanism of variant II ($z_S = 9$) as a function of the rotor rotration angle α_R. They were determined from the CAD documentation of the mechanism and calculated according to the known formula (39). The relative differences between the values of these areas are also shown in Fig. 10 and are calculated as:

$$\delta A_{ch-k.f} = \left(\frac{A_{ch-k.f}}{A_{ch}} - 1\right) \cdot 100 \tag{41}$$

The above formula is a general formula for all considered areas (as in Fig. 7). So, for example, for the area "P" type, instead of A_{ch} will be $A_{ch\text{-}P}$ and instead of $A_{ch\text{-}k.f.}$ will be $A_{ch\text{-}P\text{-}k.f.}$ e.t.c.

The above characteristics show that the use of formula (39) causes an underestimation of the value of the chamber volume by up to 3.3% in the case of a toothed chamber and 3% in the case of a non-toothed chamber. Therefore, it is advisable to look for new formulas that give a smaller error.

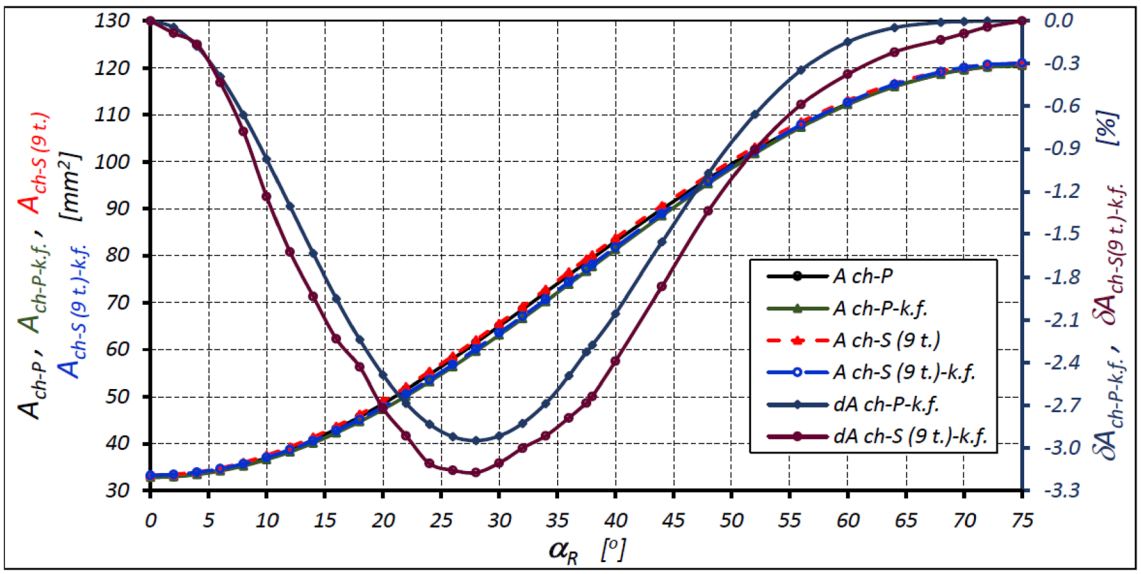

Figure 10. Areas A_{ch} of the working chamber of the satellite mechanism of variant II with the nine-tooth satellite ($z_S = 9$) as a function of the angle α_R of the rotor rotation calculated according to the known formula (39) and the relative differences of these areas: $A_{ch\text{-}P}$ – the area of the working chamber determined by the pitch line of the rotor, the curvature and the satellites; $A_{ch\text{-}S\ (9\ t.)}$ – the area of the toothed chamber; $A_{ch\text{-}P\text{-}k.f.}$ – calculated area of the working chamber $A_{ch\text{-}P}$; $A_{ch\text{-}S\ (9\ t.)\text{-}k.f.}$ – calculated area of the working chamber $A_{ch\text{-}S\ (9\ t.)}$; $\delta A_{ch\text{-}P\text{-}k.f.}$ – the relative difference between the areas $A_{ch\text{-}P}$ and $A_{ch\text{-}P\text{-}k.f.}$; $\delta A_{ch\text{-}S(9\ t.)\text{-}k.f.}$ – the relative difference between the areas of the areas $A_{ch\text{-}S\ (9\ t.)}$ and $A_{ch\text{-}S(9\ t.)\text{-}k.f.}$.

Proposed models for the working chamber area

Model I

The differences in the values for the working chamber area resulting from formula (39) can be reduced by extending this formula to the following form:

$$A_{ch-n.f.I} = 0.5 \cdot \left(A_{ch-max} - A_{ch-min}\right) \cdot [1 - \cos(\alpha_R \cdot n_{CR}) + \Theta_I \cdot \sin(\alpha_R \cdot n_{CR})] + A_{ch-min} \quad (42)$$

Where θ_I is a coefficient whose value is chosen so that:

$$\left|\delta A_{ch-n.f.I-max}\right| + \left|\delta A_{ch-n.f.I-min}\right| = min. \quad (43)$$

$$\left|\delta A_{ch-n.f.I-max}\right| \leq \left|\delta A_{ch-n.f.I-min}\right| \quad (44)$$

In Table 6, the values of the coefficient and the relative differences in the working chamber area of the considered mechanism of variant II are given and calculated as follows:

$$\delta A_{ch-n.f.I} = \left(\frac{A_{ch-n.f.I}}{A_{ch}} - 1\right) \cdot 100 \quad (45)$$

The above formula is a general formula for all considered areas (as in Fig. 7). For example, the value $A_{ch\text{-}P}$ is used instead of A_{ch} and the value $A_{ch\text{-}P\text{-}n.f.I}$ is used instead of $A_{ch\text{-}n.f.I}$ for the area of type "P" e.t.c.

The characteristics of the areas calculated according to formula (42) for the satellite mechanism of variant II with the nine-tooth satellite are shown in Fig. 11.

The above characteristics show that the use of formula (42) means that the relative difference in the calculated area of the working chamber of the mechanism with a nine-tooth satellite is not more than 0.74%. A larger difference was determined for the mechanism with a fourteen-tooth satellite (0.88%—Table 6). However, for $\alpha_R = (0,18°)$ and for $\alpha_R = (45°,75°)$ the calculated value of the chamber area is greater than the real value of this area. Furthermore, in the ranga $\alpha_R = (18°,45°)$, the calculated value of the chamber area is smaller than the actual value of this area.

Mechanism		$\delta A_{ch-n.f.I-max}$	$\delta A_{ch-n.f.I-min}$	θ_I
Type "P" (non-toothed)		0.728%	− 0.728%	0.03408
$z_S = 9$	type "S"	0.741%	− 0.741%	0.03734
	type "CH"	0.702%	− 0.702%	0.03614
$z_S = 14$		0.878%	− 0.878%	0.03679

Table 6. The relative differences in % in the calculation of the chamber area of the satellite mechanism of variant II according to model I and values of the coefficient θ_I.

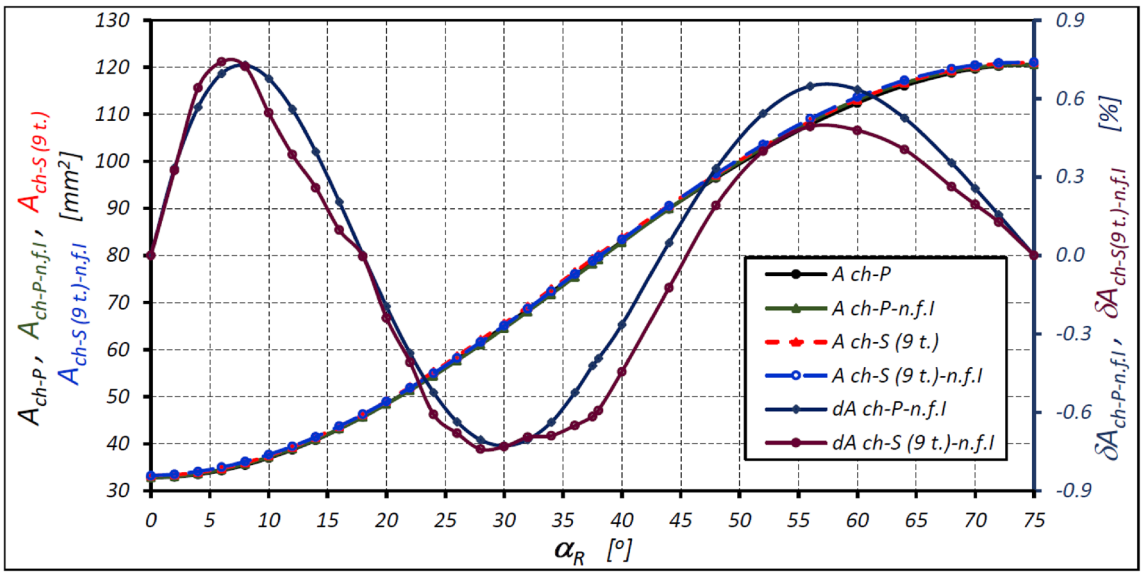

Figure 11. Areas A_{ch} of the working chamber of the satellite mechanism of variant II with nine-tooth satellite ($z_S = 9$) as a function of the angle α_R of the rotor rotation calculated according to formula (42) and the relative differences of the areas. Designations as in Fig. 10.

Model II

The differences in the values of the working chamber area resulting from formula (42) can be reduced by expanding this formula into the following form:

$$A_{ch} = 0.5 \cdot \left(A_{ch-max} - A_{ch-min}\right) \cdot [1 - \cos(\alpha_R \cdot n_{CR}) + \Theta_I \cdot \sin(\alpha_R \cdot n_{CR}) - \Theta_{II} \cdot \sin(2 \cdot \alpha_R \cdot n_R)] + A_{ch-min} \quad (46)$$

Where θ_{II} is a coefficient whose value is chosen so that conditions (43) and (44) are met.

In Table 7, the values of the coefficient Θ_{II} and the relative differences in the working chamber area of the considered mechanism of variant II are given and calculated according to formula (45). The working chamber areas were calculated according to formula (46) and the CAD documentation (as in Fig. 7).

The characteristics of the areas calculated according to formula (46) for the satellite mechanism of variant II with the nine-tooth satellite are shown in Fig. 12.

The above characteristics show that the use of formula (46) means that the relative difference in the calculated area of the working chamber of the mechanism with a nine-tooth satellite is not more than 0.63%. A larger difference was determined for the mechanism with a fourteen-tooth satellite (0.65%—Table 7).

Model III

The characteristics presented in Fig. 10 show that the greatest differences between the chamber areas calculated according to the known formula (39) and those determined from the CAD documentation occur in the middle range of the rotor rotation angle α_R. Therefore, changes can be made to the cosine function in formula (39) to obtain the minimum difference in areas. The proposed new formula is as follows:

$$A_{ch} = 0.5 \cdot \left(A_{ch-max} - A_{ch-min}\right) \cdot [1 - \cos(\alpha_{III})] + A_{ch-min} \quad (47)$$

$$\alpha_{III} = n_{CR} \cdot (\alpha_R + \Theta_{III} \cdot \sin(\alpha_R \cdot \Theta_{IV} \cdot n_{CR})) \quad (48)$$

where Θ_{III} and Θ_{IV} are coefficients whose values are chosen so that conditions (43) and (44) are satisfied.

Mechanism		$\delta A_{ch-n.f.I-max}$	$\delta A_{ch-n.f.I-min}$	Θ_{II}
type "P" (non-toothed)		0.399%	− 0.416%	0.00709
$z_S = 9$	type "S"	0.337%	− 0.630%	0.00831
	type "CH"	0.319%	− 0.392%	0.00616
$z_S = 14$		0.045%	− 0.971%	0.01096

Table 7. The relative differences in % in the calculation of the chamber area of the satellite mechanism of variant II according to model II and the values of the coefficient Θ_{II}. Coefficient Θ_I as in Table 6.

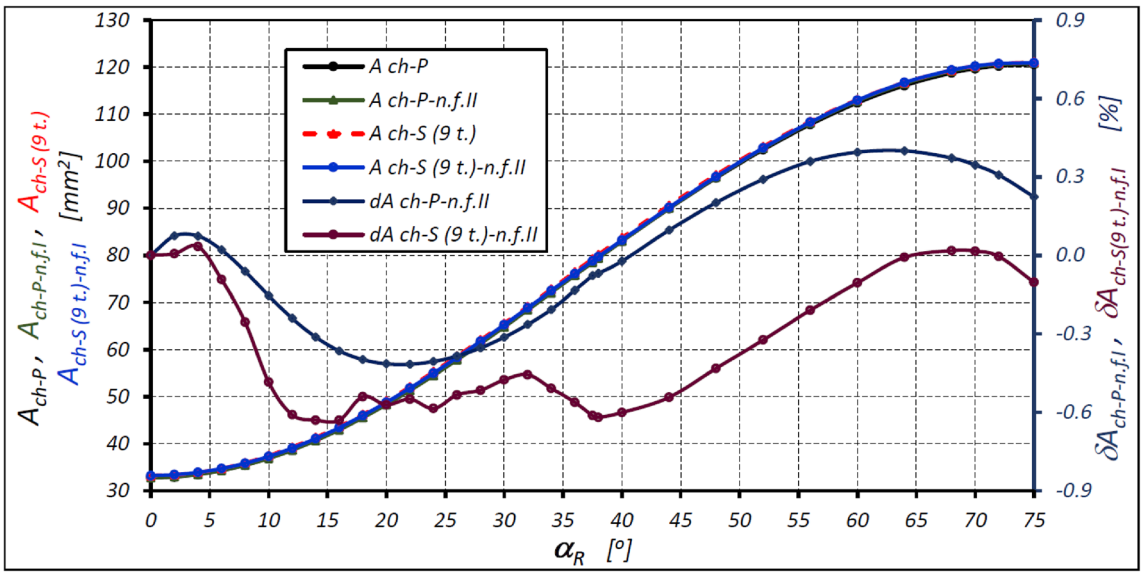

Figure 12. Areas A_{ch} of the working chamber of the satellite mechanism of variant II with nine-tooth satellite ($z_S = 9$) as a function of the angle α_R of the rotor rotation calculated according to formula (46) and the relative differences of the areas. Designations as in Fig. 10.

In Table 8, the values of the coefficients Θ_{III} and $\Theta_{II\,IV}$ and the relative differences in the working chamber area of the considered mechanism of variant II are given and calculated according to formula (45). The working chamber areas were calculated using the formula (47) and according to the CAD documentation (as in Fig. 7).

The characteristics of the areas calculated according to formula (47) for the satellite mechanism of variant II with the nine-tooth satellite are shown in Fig. 13.

The above characteristics show that the use of formula (47) means that the relative difference in the calculated area of the working chamber of the mechanism with a nine-tooth satellite is not more than 0.20% and is smaller that the difference obtained from model I. Similarly, the relative difference does not exceed 0.20% for all types of areas (Table 8).

Relative differences in the chamber area values of the toothed satellite mechanism for the coefficient values as for the non-toothed mechanism

Table 9 shows the values of the relative differences (calculated according to (45)) of the chamber area of the considered mechanism of variant II, calculated according to the models described above (formulas (39), (42), (46) and (47)) and the CAD documentation (as in Fig. 7) assuming the coefficients Θ_I, Θ_{II}, Θ_{III} and Θ_{IV} as for the non-toothed mechanism (type "P").

The comparison of the results in the table above with the results in Table 6, Table 7 and Table 8 shows that the assumption the values of the coefficients of type Θ for the toothed mechanism as for the toothless mechanism leads to an underestimation of the value of the calculated chamber area.

Conclusions

From the CAD documentation of the working mechanisms (Fig. 4) and the results contained in Table 3 and Table 5, it can be concluded that:

(a) the area of the minimum chamber of the toothed mechanism of variant I is greater than the area of the minimum chamber of the mechanism of variant II ($A_{ch\text{-}min\text{-}S\text{-}I} = 1.456 A_{ch\text{-}min\text{-}S\text{-}II}$);
(b) the area of the maximum chamber of the mechanism of variant II is smaller than the area of the maximum chamber of the mechanism variant II ($A_{ch\text{-}max\text{-}S\text{-}I} = 0.895\ A_{ch\text{-}max\text{-}S\text{-}II}$);

Mechanism		$\delta A_{ch-n.f.I-max}$	$\delta A_{ch-n.f.I-min}$	Θ_{III}	Θ_{IV}
type "P" (non-toothed)		0.152%	− 0.152%	1.0765	1.205
$z_S = 9$	type "S"	0.200%	− 0.200%	1.2160	1.145
	type "CH"	0.161%	− 0.161%	1.0861	1.170
$z_S = 14$		0.196%	− 0.196%	1.1553	1.110

Table 8. The relative differences in % in the calculation of the chamber area of the satellite mechanism of variant II according to model III and the values of the coefficients Θ_{III} and Θ_{II}.

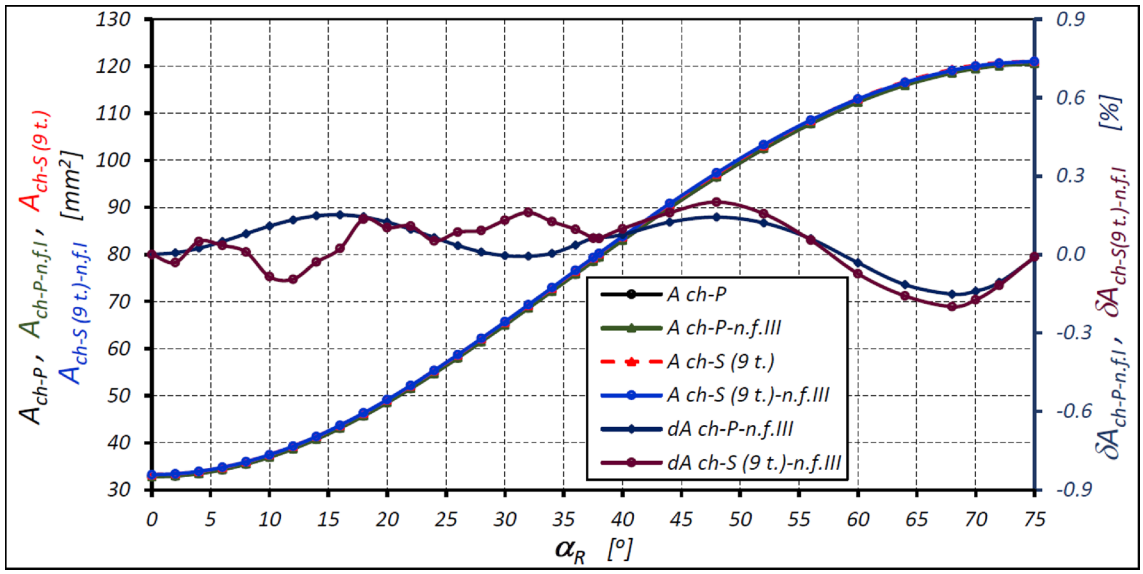

Figure 13. Areas A_{ch} of the working chamber of the satellite mechanism of variant II with nine-tooth satellite ($z_S = 9$) as a function of the angle α_R of the rotor rotation calculated according to formula (47) and the relative differences of the areas. Designations as in Fig. 10.

Model	Mechanism		Θ_I	Θ_{II}	Θ_{III}	Θ_{IV}	$\delta A_{ch-n.f.I-max}$	$\delta A_{ch-n.f.I-min}$
k.f	type "P" (non-toothed)		–	–	–	–	0	– 2.950%
	$z_S = 9$	type "S"						– 3.176%
		type "CH"						– 3.027%
	$z_S = 14$							– 3.266%
I	type "P" (non-toothed)		0.03408				0.728%	– 0.728%
	$z_S = 9$	type "S"					0.638%	– 0.954%
		type "CH"					0.618%	– 0.833%
	$z_S = 14$						0.778%	– 1.050%
II	type "P" (non-toothed)			0.00709			0.399%	– 0.416%
	$z_S = 9$	type "S"					0.072%	– 0.928%
		type "CH"					0.268%	– 0.596%
	$z_S = 14$						0.223%	– 1.291%
III	type "P" (non-toothed)		–	–	1.0765	1.205	0.152%	– 0.152%
	$z_S = 9$	type "S"					0.035%	– 0.317%
		type "CH"					0.170%	– 0.209%
	$z_S = 14$						0.198%	– 0.472%

Table 9. The relative differences in % in the calculation of the chamber area of the satellite mechanism of variant II according to all models and values of the coefficients of these models as for the non-toothed mechanism.

(c) the working volume of the mechanism of variant II is more than 46% larger than the working volume of the mechanism of variant I, because $\Delta A_{ch\text{-}S\text{-}II} = 1.465\ \Delta A_{ch\text{-}S\text{-}I}$. Therefore, the working mechanism of variant II should be used in hydraulic displacement machines (pumps and motors), as it has a favourable effect on reducing the specific mass of these machines;

(d) the $A_{ch\text{-}min}$ and $A_{ch\text{-}max}$ areas of the „S" type chamber (real toothed mechanism) differ from the areas of the "P" type chamber by up to 0.4%. Due to the fact that the toothed mechanism is used in positive displacement machines, the areas of this mechanism should be used to calculate the working volume ($A_{ch\text{-}min\text{-}S} = 1.456 A_{ch\text{-}max\text{-}S}$);

(e) in backlash-free mechanisms (the chisel is a satellite), a smaller value of both the minimum and the maximum area of the working chamber is obtained and compared to the mechanism with a classic satellite (Table 3). However, this difference is very small (less than 0.9—Table 5). Therefore, the use of backlash-free mechanisms is not justified. Another factor in favour of not using the backlash-free mechanism is the higher precision required in manufacturing and therefore the associated higher production cost;

(f) in the mechanism with a fourteen-tooth satellite, the area of both the maximum and the minimum working chambers is about 0.5% larger than the area of the chambers in the mechanism with a nine-tooth satellite (Table 3). It is therefore advisable to use a smaller number of teeth on the satellite, as a mechanism with greater tooth strength is obtained at the expense of a minimal loss of geometric working volume.

However, Fig. 9 shows that the area of the working chamber changes non-linearly from the $A_{ch\text{-}min}$ to $A_{ch\text{-}max}$ depending on the rotor rotation angle α_R. To calculate the value of the chamber area A_{ch} for any rotor rotation angle α_R, empirical formulas based on the trigonometric functions sine and cosine can be used. These are the formulas (39), (42), (46) and (47). The formula (39) is known in the literature and leads to lower calculation results for the chamber area, namely by more than 0.7% (Table 6 and Fig. 11). Lower difference values result from calculations according to the proposed formulas, i.e. formulas (42), (46) and (47). However, formula (47) provides the smallest deviations in the calculation results—no more than 0.2% (Table 8 and Fig. 13). Therefore, it is proposed to use it for the calculation of the area of the working chamber of the satellite positive displacement machine.

It is also noticeable that the number of teeth in the satellite mechanism and the tip clearances also influence its geometric working volume q_g (Table 1, Table 2, Table 3 and Fig. 6). Due to the fact that backlash-free mechanisms are not suitable for use in positive displacement machines, no further consideration is given to the working chamber areas (type "CH") of backlash-free mechanisms. However, the real mechanisms, i.e. mechanisms with areas of type "S", are not without significance. Reading the working chamber areas from the CAD documentation for different rotor rotation angles α_R is very time-consuming and sometimes problematic. It is less problematic to read the areas of the non-toothed chamber ("P" type areas). On the basis of these areas and the data (coefficients) contained in Sect. 5, the models developed above (formulae (42), (46) and (47)) can be made dependent on the number of teeth z_S of the satellite. Because model III (formula (47)) is the most accurate, considerations about models I and II are omitted. Therefore, it is proposed to write model III in the form:

$$A_{ch} = 0.5 \cdot \left(A_{ch-\max(zs)} - A_{ch-\min(zs)}\right) \cdot [1 - \cos(\alpha_{III})] + A_{ch-\min(zs)} \tag{49}$$

where:

$$\alpha_{III} = n_{CR} \cdot \left(\alpha_R + \Theta_{III(zs)} \cdot \sin\left(\alpha_R \cdot \Theta_{IV(zs)} \cdot n_{CR}\right)\right) \tag{50}$$

$$A_{ch-\min(zs)} = A_{ch-P-min} + 0.03896 \cdot z_S + 0.10836 \tag{51}$$

$$A_{ch-\max(zs)} = A_{ch-P-max} + 0.11122 \cdot z_S - 0.51258 \tag{52}$$

$$\Theta_{III(zs)} = \Theta_{III-P} - 0.01214 \cdot z_S + 0.24876 \tag{53}$$

$$\Theta_{IV(zs)} = \Theta_{IV-P} + 0.253 \cdot z_S - 2.337 \tag{54}$$

On the basis of the above formula (49) and in accordance with formula (24), the area A_{ch} of the working chamber can be calculated for:

(a) different modules of teeth of the mechanism;
(b) different number z_S of satellite teeth, provided that the shape of the pitch line of the mechanism elements is maintained (as in the case of the mechanism with a nine- and fourteen-teeth satellite considered above).

It is also possible to calculate on the basis of formula (49):

(a) the volume V_{ch} of a working chamber for each rotor rotation angle α_R;
(b) the geometric working volume q_g of the entire satellite mechanism for each rotor rotation angle α_R;
(c) the unevenness of the absorption of the satellite mechanism at constant rotor speed;
(d) the unevenness of the theoretical torque at a constant pressure difference in the working chambers of the mechanism.

The above topics will be the subject of separate publications.

Data availability

The datasets used and/or analysed during the current study are available from the corresponding author on reasonable request.

Received: 28 December 2023; Accepted: 9 May 2024
Published online: 16 May 2024

References

1. Kim, T., Kalbfleisch, P. & Ivantysynova, M. The effect of cross porting on derived displacement volume. *Int. J. Fluid Power* https://doi.org/10.1080/14399776.2014.923605 (2014).
2. Drogosz, P., Teoretyczne badanie chłonności obiegowych silników hydraulicznych (eng. Theoretical study of the absorption of circulating hydraulic motors.). Ph.D. dissertation. Poznan University of Technology (2001).
3. Sliwinski, P. Determination of the theoretical and actual working volume of a hydraulic motor. *Energies* **13**(22), 5933. https://doi.org/10.3390/en13225933 (2020).
4. Sliwinski, P. Determination of the theoretical and actual working volume of a hydraulic motor—Part II (The method based on the characteristics of effective absorbency of the motor). *Energies* **14**(6), 1648. https://doi.org/10.3390/en14061648 (2021).
5. Sliwinski, P. The influence of pressure drop on the working volume of a hydraulic motor. *Eks. Niez. Main. Rel.* https://doi.org/10.17531/ein.2022.4.15 (2022).
6. Garcia-Bravo J. & Nicholson J.: What is the real size of that pump? Fluid Power Journal, 2018. Available online: https://fluidpowerjournal.com/real-size-pump/ (Accessed on 15 December 2023).
7. Osinski, P., Deptula, A. & Partyka, M. Hydraulic tests of the PZ0 gear micropump and the importance rank of its design and operating parameters. *Energies* **15**(9), 3068. https://doi.org/10.3390/en15093068 (2022).
8. Kollek, W., Osinski, P., Stosiak, M., Wilczynski, A. & Cichon, P. Problems relating to high-pressure gear micropumps. *Arch. Civ. Mech. Eng.* https://doi.org/10.1016/j.acme.2013.03.005 (2014).
9. Kollek, W. & Radziwanowska, U. Energetic efficiency of gear micropumps. *Arch. Civ. Mech. Eng.* https://doi.org/10.1016/j.acme.2014.05.005 (2015).
10. Zaluski, P. Influence of fluid compressibility and movements of the swash plate axis of rotation on the volumetric efficiency of axial piston pumps. *Energies* **15**(1), 298. https://doi.org/10.3390/en15010298 (2022).
11. Stawinski, L., Kosucki, A., Cebulak, M., Gorski, G. V. & Grala, A. M. Investigation of the influence of hydraulic oil temperature on the variable-speed pump performance. *Eksp. Niez. Maint. Rel.* https://doi.org/10.1753/ein.2022.2.10 (2022).
12. Zardin, B., Natali, E. & Borghi, M. Evaluation of the hydro-mechanical ffficiency of external gear pumps. *Energies* **12**(13), 2468. https://doi.org/10.3390/en12132468 (2019).
13. Manring, N. & Williamson, C. The theoretical volumetric displacement of a check-valve type, digital displacement pump. *J. Dyn. Sys. Meas. Control* https://doi.org/10.1115/1.4041713 (2019).
14. Kujawski, M. Metody wyznaczania głównych parametrów eksploatacyjnych obiegowych silników hydraulicznych z nieokrągłymi kołami zębatymi (eng. Methods for determining the main operating parameters of circulating hydraulic motors with non-circular gears). *Hyd. Pneum.* **1** (1996).
15. Kujawski, M., Ustalenie ogólnych równań i algorytmu ich rozwiązywania w celu wyznaczenia chłonności właściwej obiegowych silników hydraulicznych (eng. Determine the general equations and their solution algorithm for determining the specific absorption of circulating hydraulic motors). Maszyny Górnicze 70 (1997).
16. Drogosz, P.: Weryfikacja analitycznej metody wyznaczania chłonności właściwej silników obiegowo krzywkowych (eng. Verification of the analytical method for determining the specific absorption of circulating motors). *Masz. Gor.* **67** (1997).
17. Drogosz, P., Kujawski, M: Chłonność właściwa różnych odmian obiegowych silników hydraulicznych (eng. Specific absorption of different varieties of circulating hydraulic motors). *Masz. Gor.* **75** (1998).

18. Sliwinski, P. *Satelitowe maszyny wyporowe. Podstawy projektowania i Analiza strat energetycznych* (eng. *Satellite displacement machines. Basic of design and analysis of power loss*). (Gdansk University of Technology Publishers, Gdansk, Poland, 2016).
19. Sliwinski, P. The methodology of design of satellite working mechanism of positive displacement machine. *Sci. Rep.* **12**, 13685. https://doi.org/10.1038/s41598-022-18093-z (2022).
20. Sliwinski, P. Influence of geometrical and operational parameters on tooth wear in the working mechanism of a satellite motor. *Sci. Rep.* **13**, 17028. https://doi.org/10.1038/s41598-023-44319-9 (2023).
21. Sliwinski, P., Patrosz, P. Satelitowy mechanizm roboczy hydraulicznej maszyny wyporowej (eng. Satellite operating mechanism of the hydraulic displacement machine). Patent PL 218888. https://ewyszukiwarka.pue.uprp.gov.pl/search/pwp-details/P.401821 (2015).
22. Sliwinski, P., Mechanizm satelitowy hydraulicznej maszyny wyporowej (Satellite operating mechanism of a hydraulic displacement machine). Patent application https://ewyszukiwarka.pue.uprp.gov.pl/search/pwp-details/P.437751 (2021).
23. Sliwinski, P: Mechanizm satelitowy hydraulicznej maszyny wyporowej (Satellite operating mechanism of a hydraulic displacement machine). Patent application P.445212 (2023).
24. Luan, Z. & Ding, M. Research on non-circular planetary gear pump. *Adv. Mat. Res.* https://doi.org/10.4028/www.scientific.net/AMR.339.140 (2011).
25. Li, D., Liu, Y., Gong, J. & Wang, T. Design of a noncircular planetary gear mechanism for hydraulic motor. *Mat. Prob. Eng.* **2021**, 5510521. https://doi.org/10.1155/2021/5510521 (2021).
26. Zhang, B., Song, S., Jing, C. & Xiang, D. Displacement prediction and optimization of a non-circular planetary gear hydraulic motor. *Adv. Mech. Eng.* https://doi.org/10.1177/16878140211062690 (2021).
27. Brzeski, J., Sieniawski, B., Ostrowski, J. Silnik hydrauliczny obiegowo-krzywkowy (eng. Rotary-cam hydraulic motor). Patent PL 105317, https://ewyszukiwarka.pue.uprp.gov.pl/search/pwp-details/P.195349?lng=pl (1977).
28. Sieniawski, B. Silnik hydrauliczny obiegowo-krzywkowy (eng. Rotary-cam hydraulic motor). Patent PL 71329, https://ewyszukiwarka.pue.uprp.gov.pl/search/pwp-details/P.151883?lng=pl (1974).
29. Sieniawski, B., Potulski, H. & Sieniawski, D. Silnik obiegowo-krzywkowy, zwłaszcza jako silnik hydrauliczny (eng. Rotary-cam motor, especially as a hydraulic motor). Patent PL 146450, https://ewyszukiwarka.pue.uprp.gov.pl/search/pwp-details/P.251543?lng=pl (1985).
30. JianGang, L., XuTang, W. & ShiMin, M. Numerical computing method of noncircular gear tooth profiles generated by shaper cutters. *Int. J. Adv. Man. Tech.* https://doi.org/10.1007/s00170-006-0560-0 (2007).
31. Dietrich, M. *Podstawy konstrukcji maszyn. eng Fundamentals of machine design* Vol. 2 (PWN Publishing House, 2022).
32. Sieniawski, B. Satelitowa maszyna wyporowa (eng. Satellite displacement machine). Patent PL 216648, https://ewyszukiwarka.pue.uprp.gov.pl/search/pwp-details/P.391060 (2010).
33. Sieniawski, B., Skorynkiewicz S.: Silnik hydrauliczny obiegowo-krzywkowy (Hydraulic planetary gear motor). Patent PL 212435. https://ewyszukiwarka.pue.uprp.gov.pl/search/pwp-details/P.385828 (2012).
34. Sakama, S., Tanaka, Y. & Kamimura, A. Characteristics of hydraulic and electric servo motors. *Actuators* **11**(1), 11. https://doi.org/10.3390/act11010011 (2022).
35. Hemmi, M. Morita, R., Hirota, Y., Inoue, K., Nabae, H., Endo, G. & Suzumori, K.: Development of hydraulic tough motors with high power density and their application to a 7-axis robotic arm. *2019 IEEE/SICE International Symposium on System Integration (SII)*, Paris, France. https://doi.org/10.1109/SII.2019.8700419 (2019).
36. Holling, G. High-power density motors. Rocky Mountain Technologies, https://www.powertransmission.com/articles/1346-high-power-density-motors (Access date: 19.12.2023).
37. Catalog of piston hydraulic motors serie MSI of Hydro-Leduc company, https://www.hektos.eu/pdfdocs/MSI_PL_net.pdf (Access date: 19.12.2023).
38. Catalog of satellite motors of SM-Hydro company, https://smhydro.com.pl (Access date: 19.12.2023).
39. Catalog of satellite motors of PONAR company, https://www.ponar-wadowice.pl/en/n/new-product-satellite-motors (Access date: 19.12.2023).

Author contributions

The manuscript was written entirely by the author.

Competing interests

The author declares no competing interests.

Additional information

Correspondence and requests for materials should be addressed to P.S.

Reprints and permissions information is available at www.nature.com/reprints.

Publisher's note Springer Nature remains neutral with regard to jurisdictional claims in published maps and institutional affiliations.